Bioorganic & Medicinal Chemistry 19 (2011) 3769–3776

Contents lists available at ScienceDirect

Bioorganic & Medicinal Chemistry

journal homepage: www.elsevier.com/locate/bmc

Characterization of chemical, radiochemical and optical properties of a dual-labeled MMP-9 targeting peptide

Ali Azhdarinia [a,*], Nathaniel Wilganowski [a], Holly Robinson [a], Pradip Ghosh [a], Sunkuk Kwon [a], ZaWaunyka W. Lazard [b], Alan R. Davis [b], Elizabeth Olmsted-Davis [b], Eva M. Sevick-Muraca [a]

[a] Center for Molecular Imaging, The Brown Foundation Institute of Molecular Medicine, The University of Texas Health Science Center, Houston, TX 77030, USA
[b] Center for Cell and Gene Therapy, Baylor College of Medicine, One Baylor Plaza MS BCM505, Houston, TX 77030, USA

ARTICLE INFO

Article history:
Received 22 February 2011
Revised 25 April 2011
Accepted 30 April 2011
Available online 6 May 2011

Keywords:
Dual-labeling
Near-infrared fluorescence
Gallium-68
MMP

ABSTRACT

Optical imaging possesses similar sensitivity to nuclear imaging and has led to the emergence of multimodal approaches with dual-labeled nuclear/near-infrared (NIR) agents. The growing impact of ^{68}Ga ($t_{1/2}$ = 68 min) labeled peptides on preclinical and clinical research offers a promising opportunity to merge the high spatial resolution of NIR imaging with the clinically-accepted positron emission tomography (PET). Previously, dual-labeled agents have been prepared with longer-lived radiometals and showed no detrimental effects on optical properties as a result of radiolabeling. In this study, we selected a peptide (M_2) that targets MMP-2/9 and is dual-labeled with IRDye 800CW and ^{68}Ga. Since ^{68}Ga chelation typically requires low pH (3.5–4) and elevated heating temperatures (95 °C), we sought to evaluate the impact of ^{68}Ga labeling on the optical properties of M_2. An efficient method for preparation of ^{68}Ga-M_2 was developed and reaction conditions were optimized. Stability studies in PBS, DTPA, and serum were performed and high levels of intact agent were evident under each condition. The addition of multiple reporters to a targeting agent adds further complexity to the characterization and validation and thus requires not only testing to ensure the agent is stable chemically and radiochemically, but also optically. Therefore, fluorescence properties were evaluated using a spectrofluorometer as well as by fluorescence detection via HPLC. It was determined that ^{68}Ga-labeling conditions did not impair the fluorescent properties of the agent. The agent was then used for in vivo imaging in a mouse model of heterotopic ossification (HO) with activated MMP-9 expression as an early biomarker which precedes mineralization. Although ^{68}Ga-complexation greatly reduced binding affinity of the peptide and negated tracer uptake on PET, NIR imaging showed consistent fluorescent signal that correlated to MMP-9 expression. This attests to the feasibility of using ^{68}Ga/NIR for dual-labeling of other peptides or small molecules for multimodality molecular imaging.

1. Introduction

Multimodality imaging provides complementary functional and anatomical information for diagnosis, treatment planning, and therapeutic monitoring. Clinical hybrid systems that combine functional imaging modalities such as Positron Emission Tomography (PET) and Single-Photon Emission Computed Tomography (SPECT) with Computed Tomography (CT) offer the ability to obtain molecular imaging data that can be co-registered with anatomical imaging, playing substantial roles in patient care. The development of a single agent capable of carrying dual-contrast for both nuclear and CT or MRI imaging modalities proves challenging due to the inherent differences in measurement sensitivities between nuclear and all other conventional imaging modalities. While the pico- to femto- molar sensitivity of nuclear imaging permits the use of microdosing and minimizes potential pharmacologic effects and toxicity of a radiotracer, MR and CT contrast agents currently require millimolar tissue concentrations for acquisition.[1]

Near-infrared fluorescence (NIRF) optical imaging is an emerging imaging modality that promises comparable sensitivity to nuclear imaging.[2,3] Because of the comparable sensitivity, dual optical/nuclear labeling of molecularly-targeted imaging agents can provide specific advantages. Foremost, if an imaging agent can be dual-labeled with a radionuclide and a NIR excitable fluorophore, then a single imaging agent can be used for non-invasive imaging of diseased tissues (via PET and possibly NIRF imaging) as well as intraoperative guidance for accurate surgical removal of corresponding tissues and tissue margins (via NIR fluorescence

* Corresponding author. Address: Center for Molecular Imaging, SRB 330C, 1825 Pressler Street, The Brown Foundation Institute of Molecular Medicine, University of Texas Health Science Center, Houston, TX 77030, USA. Tel.: +1 713 500 3577; fax: +1 713 500 0319.
E-mail address: ali.azhdarinia@uth.tmc.edu (A. Azhdarinia).

0968-0896/$ - see front matter © 2011 Elsevier Ltd. All rights reserved.
doi:10.1016/j.bmc.2011.04.054

imaging). Second, because the NIR signal does not have a physical half-life, it can facilitate the validation of agent targeting capabilities long after physical decay of radiotracer. Lastly, if NIR fluorescent agents are to be used in molecular imaging, dual-labeling provides a strategy for comparative assessment against the conventional nuclear imaging modalities.

To date, the only NIR fluorophore that has been employed in human NIRF imaging studies is indocyanine green (ICG).[4] However, dyes that possess better optical properties (i.e., increased fluorescent yield, preferable hydrophilicity, and enhanced stability) and can be subjected to reaction in organic, aqueous and solid phase chemistries with reduced risk of physical degradation or loss of fluorescence following radiolabeling are of great interest. IRDye 800CW is a NIR dye functionalized with either an *N*-hydroxysuccinimide or maleimide reactive group, allowing it to be attached to a number of biomolecules. Owing to its NIR excitation which abrogates tissue autofluorescence as a complicating background signal[5] as well as to its unprecedented stability, IRDye 800CW has been used in a number of preclinical studies.[6–12] While the imaging sensitivity to IRDye 800CW and other NIR fluorophores ultimately depends upon instrumentation design,[3] efficiency of dual-labeled agents also depends upon the stability and efficient fluorescent yield of the NIR fluorophore following conjugation and radiolabeling.

Different nuclear/optical dual-labeling strategies have been reported for antibody[6,7,13,14] and peptide-based agents.[15–19] Our previous experiences with dual-labeled agents were with antibodies and required longer-lived radionuclides, such as ^{64}Cu ($t_{1/2}$ = 12.7 h) and ^{111}In ($t_{1/2}$ = 2.8 d), to allow for sufficient clearance from background tissues and permit imaging at delayed time points (i.e., 24 h). We and others are also developing peptide agents as they are ideal molecules for dual-labeling since they can be synthesized by solid phase peptide synthesis and have a clearly defined structure to which site-specific conjugations can be performed. Also, peptides clear rapidly from circulation and provide high target-to-background ratios at early time points. Our initial studies with dual-labeled peptides used ^{64}Cu to allow for longitudinal PET imaging at early and delayed time points to monitor distribution, clearance routes, agent stability, and determine the optimal time point for imaging. Due to limitations in

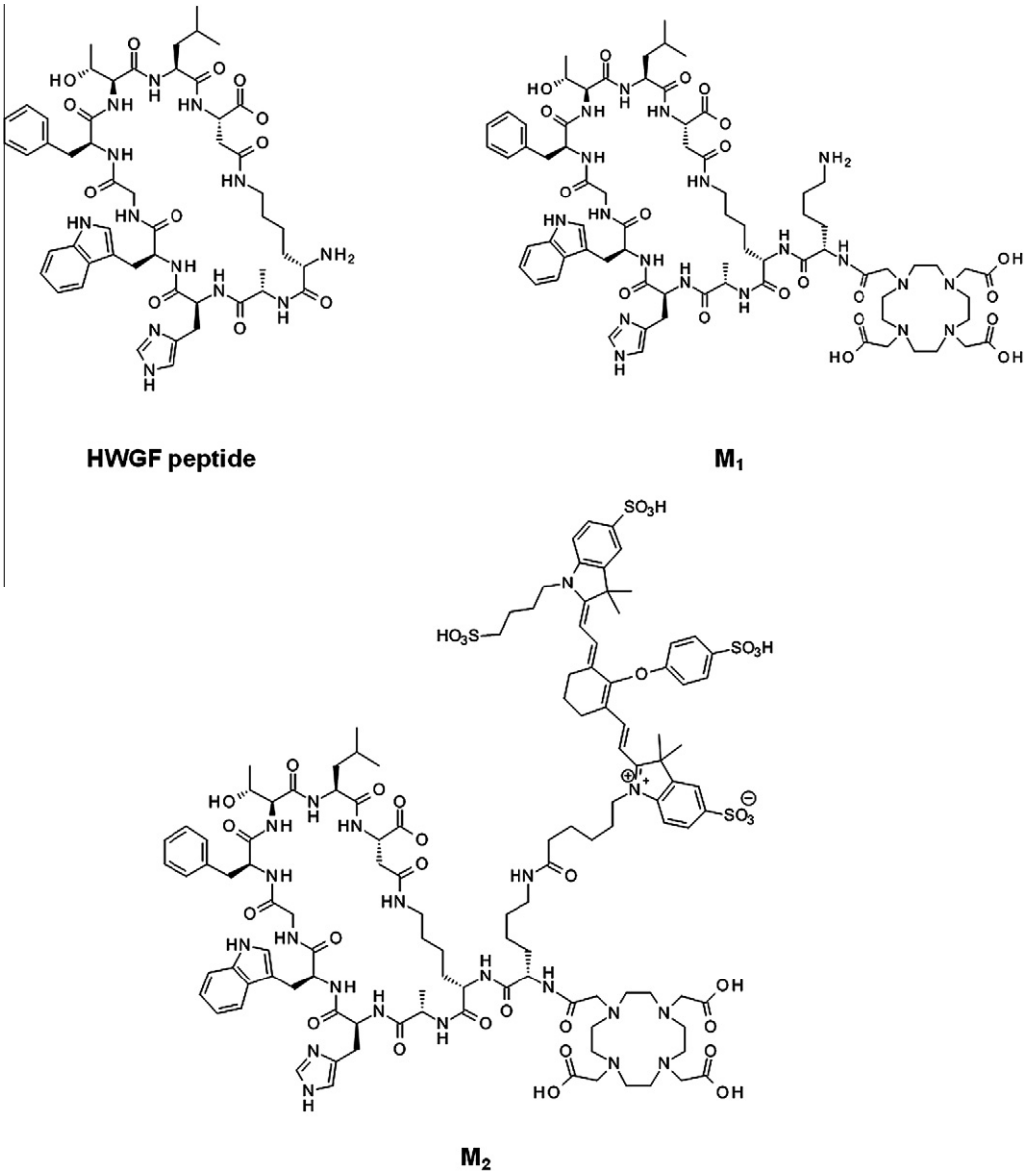

Figure 1. Chemical structures of HWGF peptide, DOTA-derivatized peptide (M_1) and dual-conjugate (M_2).

the production of ^{64}Cu, we explored the use of more readily-available PET radionuclides, such as ^{68}Ga, which possesses a shorter half-life (68 min) and is widely-used for peptide imaging. ^{68}Ga is a positron-emitting radionuclide produced from commercially-available generators. Since the generator is housed locally and can be eluted multiple times per day, it allows for rapid method development and clinical deployment of new radiotracers. ^{68}Ga is formed as the decay product of the long-lived parent radionuclide Germanium-68 (^{68}Ge, $t_{1/2}$ = 270 d), thus allowing routine use of the ^{68}Ga-generator for nearly one year.

In this study, we evaluated the feasibility of using a ^{68}Ga/IRDye 800CW dual-labeling strategy for a peptide that targets the gelatinases, matrix metalloproteinases-2 and -9 (MMP-2/-9). MMPs are a family of enzymes that participate in extracellular matrix (ECM) degradation. Altered MMP expression has been reported in physiological conditions including rheumatoid arthritis, atherosclerosis, heart failure, pulmonary emphysema, and tumor growth and metastasis, and bone formation.[20–25] A model of heterotopic ossification (HO) has been described using bone morphogenetic protein (BMP) signaling which activates MMP-9 and contributes to the new bone formation.[26] While there are several strategies for targeting the entire family of MMPs, Koivunen et al. originally described several peptide sequences containing the HWGF motif that showed excellent inhibition of the gelatinases, MMP-2 and MMP-9.[27] The CTTHWGFTLC (CTT) peptide showed the best inhibitory properties and led to its functionalization by others to generate different imaging probes with Iodine-125 (^{125}I), Indium-111 (^{111}In), and Copper-64 (^{64}Cu) labels.[28–30] In an attempt to generate a variant of the CTT peptide for fluorescence imaging, Wang et al. modified the N-terminus in order to attach a red-excitable fluorophore, Cy5.5, and to improve the in vivo stability of the peptide.[31] This agent showed specific tumor uptake and served as the basis for the NIR/PET dual-labeled compound shown in Figure 1.

2. Results

2.1. Conjugation of IRDye 800CW

The dual-conjugate M_2 was formed through attachment of IRDye 800CW to M_1. Analysis of the spin column-purified sample by HPLC showed >90% purity with a small amount of unreacted M_1 present in the final product and was used for all subsequent studies. Figure 2 shows HPLC chromatograms with UV detection at 280 nm and fluorescence detection. Retention times of 5.9 min and 6.1 min were observed for M_1 and M_2 (at 280 nm), respectively, while fluorescence detection of IRDye 800CW had a retention time of 5.6 min. The HPLC data shows a single fluorescent peak for M_2, confirming formation and purity of the dual-conjugate. Analysis by ESI-MS showed that the observed molecular weight (2555.9) was in excellent agreement with the calculated value (2555.92).

2.2. MMP-9 binding assays

HWGF-peptides described by Wang et al. were further modified by DOTA and IRDye 800CW conjugation and enzyme binding was evaluated. Binding of M_2 with MMP-9 could be visualized with 400 nM peptide, whereas a 10-fold increase in concentration of processed M_2 was required for detection (Fig. 3A and B). This indicates a detrimental effect from the labeling conditions which may be mainly due to the elevated heat required for Ga complexation by DOTA. ^{nat}Ga-M_2 binding occurred at concentrations >400 μM (data not shown) showing an even further reduction in binding affinity. In blocking studies, a 200 μM concentration of M_1 was needed to produce a modest decrease in M_2 signal and substantial inhibition was only observed at concentrations >1 mM (Fig. 3C), thus no further steps were taken to remove the small amounts of ^{68}Ga-M_1 from the radiolabeled product.

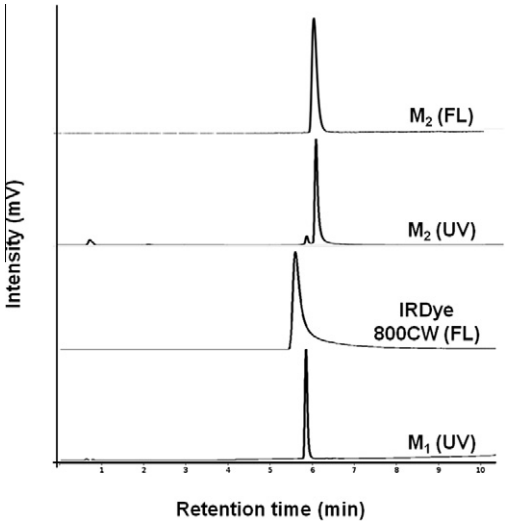

Figure 2. HPLC traces for M_1, IRDye 800CW and M_2. Traces were acquired at 280 nm or with a fluorescence detector.

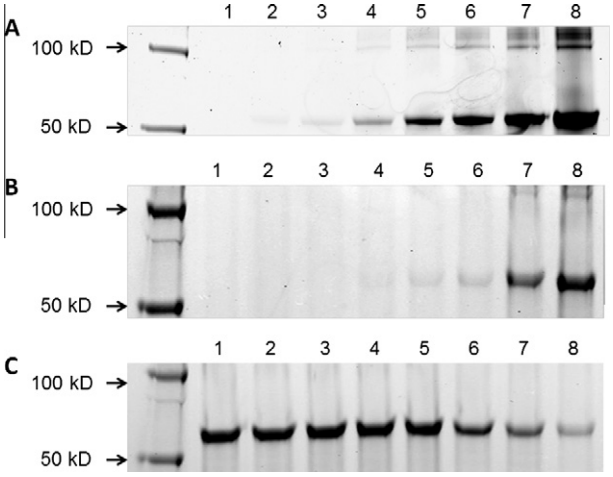

Figure 3. MMP-9 enzyme binding assays. Shown are the fluorescent scans acquired on the LICOR infrared imaging system. In all cases, 10 ng of purified MMP-9 was used and binding was resolved by SDS gel electrophoresis. The binding experiments shown are as follows: MMP-9 was incubated with increasing amounts of M_2 (A) and processed M_2 (B) at concentrations of 0, 0.1, 0.2, 0.4, 1, 2, 4 and 10 μM (lanes 1–8). For the blocking study (C), MMP-9 was incubated with M_1 at concentrations of 0.2, 0.5, 1, 2, 20, 200, 500 and 1000 μM (lanes 1–8). M_2 (2 μM) was then added and incubated for 1 h. Bands resolved at 62 kDa correspond to M_2 binding with MMP-9.

2.3. Radiochemistry

M_2 was radiolabeled with ^{68}Ga using the fractionation method and radiochemical purity (RCP) of >95% were achieved within 10 min, with 13 min selected as the optimal heating time. ^{68}Ga-M_2 was formed with high labeling efficiency over the range of peptide amounts investigated. Similar RCP were observed between the peptide amounts tested, therefore, 6 nmol (15 μg) was selected for radiolabeling experiments to achieve the highest specific activity and reaction conditions were optimized using 0.1 N NaOAc buffer. A specific activity of 42 Ci/mmol was used for imaging studies to ensure sufficient NIR signal. Co-injection

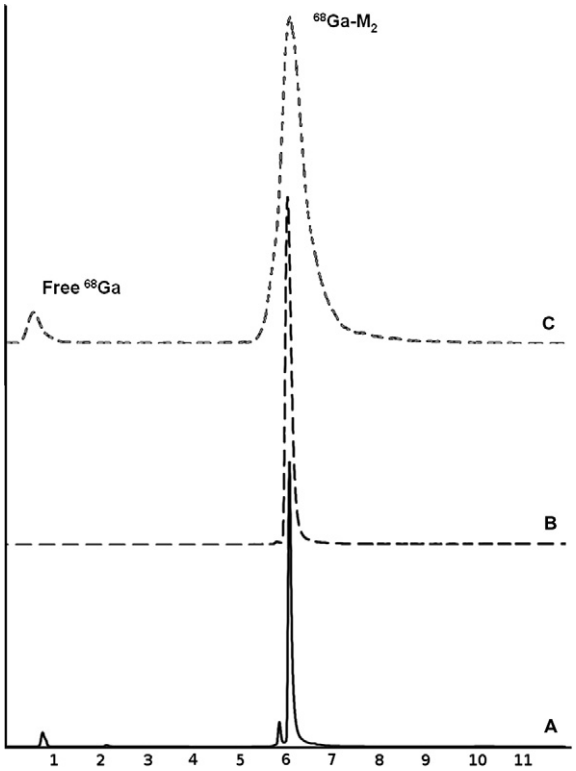

Figure 4. HPLC chromatograms for ^{68}Ga-M$_2$: UV at 280 nm (A), fluorescent (B), and radiometric (C).

of ^{nat}Ga-M$_2$ and ^{68}Ga-M$_2$ on HPLC showed excellent correlation between the UV, fluorescent, and radiometric peaks (Fig. 4). The log *P* value for ^{68}Ga-M$_2$ was calculated to be −2.09 ± 0.02.

2.4. Stability studies

Peptide and optical stability were evaluated in water and PBS at 4 °C and room temperature. Over the 14 day incubation period, HPLC analysis revealed no significant degradation of peptide or fluorescent signal. Retention times were consistent and peak values did not significantly change based on quantitation from the HPLC fluorescence detector. The effects of Ga-labeling conditions on the fluorescent properties of M$_2$ were evaluated using radioactive and ^{nat}Ga and showed no deterioration in fluorescence signal of the dual-labeled agent. ^{68}Ga-M$_2$was stable in PBS, DTPA and mouse serum as indicated by >95% radiochemical purity at 3 h incubation (Fig. 5).

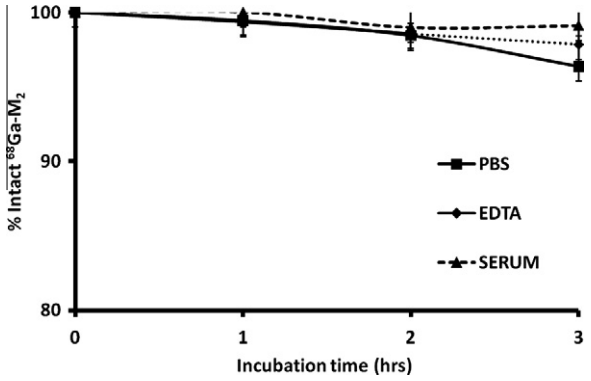

Figure 5. Stability studies for ^{68}Ga-M$_2$ in PBS, DTPA challenge and serum.

Table 1
Spectral properties of NIR and dual-labeled agents[a]

Sample	Excitation/emission wavelength (nm)	Extinction coefficient (M^{-1} cm^{-1})	Quantum yield[b]
IRDye 800CW	785/830	181,458 ± 2189	0.034
M$_2$	785/830	160,053 ± 3802	0.034
^{68}Ga-M$_2$	785/830	108,069 ± 7918	0.031

[a] Data presented as mean ± standard deviation (n = 4).
[b] The fluorescence quantum yield (Φ) was measured using an aqueous solution of ICG (Φ = 0.016).

2.5. Fluorescent properties

Table 1 shows a summary of the spectral properties of IRDye 800CW, M$_2$ and ^{68}Ga-M$_2$. The optical spectrum of M$_2$ exhibited an absorbance maximum at 785 nm with an average extinction coefficient of 160,530 ± 3802 M^{-1} cm^{-1} which is similar to that calculated for IRDye 800CW. Similarly, ^{68}Ga-M$_2$ showed maximum absorbance at 785 nm but reported a lower extinction coefficient value of 108,069 ± 7918 M^{-1} cm^{-1}. Using an excitation wavelength of 785 nm, M$_2$ and ^{68}Ga-M$_2$ demonstrated fluorescence quantum yields (Φ) of 0.034 and 0.031, respectively, relative to ICG. These values were in reasonable agreement with the calculated quantum yield of IRDye 800CW (Φ = 0.034) and attests to the efficiency of these IRDye 800-based peptide conjugates.

2.6. Quantitation of BMP2 protein and activity

We have characterized BMP-2 expression from the adenovirus transduced cells in vitro and shown expression level as compared to control cells (Fig. 6). W20-17 cells, a mouse bone marrow stem cell line, have increased alkaline phosphatase (AP) activity in response to BMP-2 treatment which corresponds to osteogenic differentiation of cells and BMP-2 functional activity in vitro. Using the known concentrations of BMP-2 with their corresponding AP activity readings, the transduced MRC5 cells had significantly more BMP-2 protein (0.74 ng) in comparison to the control cells (0.19 ng) (p <0.0005).

2.7. In vivo imaging

Figure 7A and C presents typical NIR fluorescence images of mice at four days after implantation. The images were taken 18 h post-injection of ^{68}Ga-M$_2$ and show the dorsal view of mice with right hind limbs injected with AdBMP2 cells (solid arrows) and the left hind limbs injected with Adempty cells (dashed arrows). Localization of ^{68}Ga-M$_2$ was observed in the tissue region with BMP-2 producing cells with minimal fluorescence detected in the contralateral region. Figure 7B and D shows CTs acquired for each

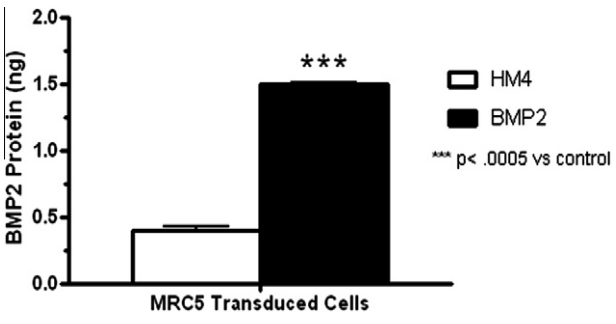

Figure 6. In vitro characterization of BMP-2 expression from adenovirus transduced cells.

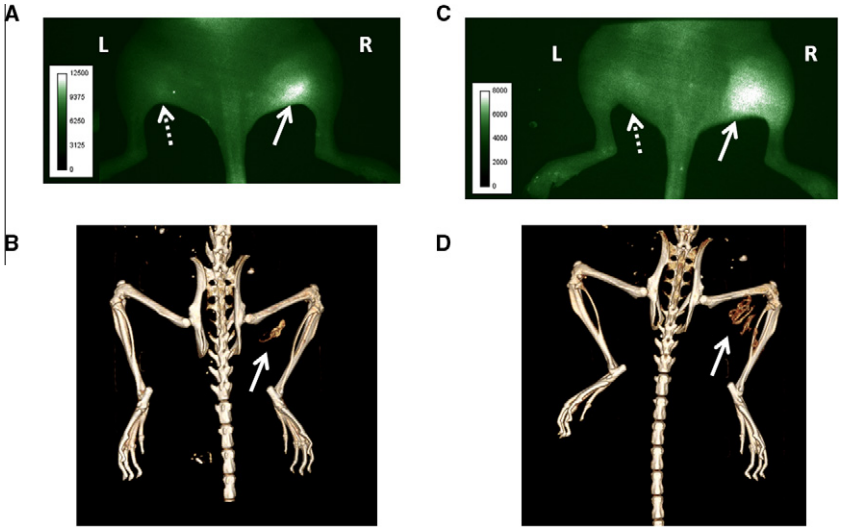

Figure 7. Multimodality imaging of mice with fracture putty implants. Human fibroblast cells transduced with AdBMP2 were injected into the right hind limb of NOD/SCID mice. Mice were injected with ^{68}Ga-M_2 and imaged at 18 h. NIR images (A and C) were acquired on day four post-implantation and follow-up CTs (B and D) were taken on day 11. Solid arrows indicate site of new bone formation and agent accumulation. Dashed arrows designate control (empty cassette) injection sites in the contralateral limb.

mouse on day 11 post-implantation and provide evidence of new bone formation at the site corresponding to agent uptake on the NIR images. The findings demonstrate the feasibility of NIR imaging following ^{68}Ga-labeling with consistent fluorescent signal obtained in all cases, and also indicate the mechanism of tracer accumulation may be related to MMP-9 expression during HO. In contrast with previous results using ^{64}Cu-M_2,[26] PET imaging of ^{68}Ga-M_2 was confounded by the overwhelming signal from the nearby bladder and showed only negligible uptake at the target site (data not shown). Nonetheless, mouse imaging shows that in vivo NIR signal and targeting of MMP-9 was not perturbed by ^{68}Ga labeling.

3. Discussion

The use of hybrid imaging has gained acceptance clinically led by the advent and utility of combining the functional imaging of nuclear imaging with anatomical correlation by CT, and more recently with the introduction of PET/MRI. In the case of cancer, multimodal imaging platforms have improved diagnosis through co-registration of images, providing physicians with methods to identify lesions with better certainty and accuracy and tailor treatment strategies.[32,33] As a result, tumors can be detected earlier and therapeutic intervention can be initiated prior to reaching advanced stages of the disease. An even further extension of multimodal imaging applications is intraoperative use for image-guided surgery by combining PET/NIR into a single agent. For example, an agent can be dual-labeled with a radionuclide and a NIR fluorophore and injected a day prior to surgery for PET/CT imaging for lesion detection and surgical planning. On the following day, the radioactivity will have decayed and the surgeon can remove the tumor using conventional methods, but could now incorporate intraoperative optical imaging to detect any existing NIR signal from residual tumor tissue. This directly permits visualization of any positive margins that still remain via molecular imaging and guides the surgeon on the potential need for further surgical intervention in real-time.

Since the sensitivities of CT and MRI are far lower than nuclear modalities, the design of agents bearing beacons for both nuclear and anatomical imaging is challenging. Conversely, optical imaging possesses similar sensitivity to nuclear imaging and the feasibility of a multimodality imaging approach with dual-labeled nuclear/NIR peptides has been described in a recent review.[34] We have previously shown that dual-labeling of antibodies with a radionuclide and a NIR fluorophore can be achieved using various combinations of IRDye 800CW and metal chelates with either ^{111}In or ^{64}Cu.[6,7,14] In the case of antibodies, it is known that extended plasma circulation times are critical for therapy as they reduce the need for frequent dosing. However, for imaging this creates high levels of radioactivity present in the blood and liver and mandates later imaging time points to achieve lower background levels and sufficient contrast. Longer-lived radionuclides such as ^{111}In and ^{64}Cu allow for delayed imaging and clearing of the agent from circulation. Thus, these radiometals are widely-used for antibody imaging and have been adopted in many dual-labeling strategies.

Peptides are of particular importance in molecular imaging due to favorable pharmacokinetic properties, specific interaction with cell surface receptors, preparation in high specific activities, and robust manufacturing schemes by solid phase synthesis. The tendency of peptides to rapidly associate with receptors and clear from non-target sites permits imaging at early time points through the use of shorter-lived radionuclides such as ^{68}Ga. As such, the use of ^{68}Ga-peptides has experienced tremendous growth over the past decade.[35–37] Since previous reports with dual-labeled nuclear/NIR agents predominantly used ^{64}Cu or ^{111}In, we examined the potential role of ^{68}Ga in dual-labeling primarily because of the availability of the generator systems and the possibility of imaging at earlier time points due to the rapid clearance of ^{68}Ga-tracers. Also, since ^{64}Cu and ^{111}In have milder radiolabeling conditions (pH >5, heat at rt–80 °C) than ^{68}Ga (pH 3.5–4, heat at 80–98 °C for DOTA chelates), we sought to examine the effects of ^{68}Ga labeling conditions on the optical properties of IRDye 800CW. Multiple ^{68}Ga labeling schemes have been reported which minimize the effect of ^{68}Ge breakthrough and concentrate the generator eluate through fractionation or ion exchange methods, but a common thread shared by most DOTA-based schemes is the need to label in acidic conditions with elevated heating.[38–41] Thus, we explored these effects on M_2 to evaluate chemical and optical stability in response to ^{68}Ga labeling using a modified version of the method described by Breeman et al.[39]

The two-week stability study of M_2 revealed no degradation of peptide or fluorescent signal at 4 °C or room temperature. Initially, care was taken to shield samples from light, but the data showed no added benefit as samples exposed to ambient light showed

identical fluorescent intensity by HPLC analysis. The stability of the dye was further confirmed when M_2 was labeled with $^{68}Ga/^{nat}Ga$ and showed no alteration in fluorescence profile. Optical properties were assessed for IRDye 800CW, M_2 and ^{68}Ga-M_2 and showed minor changes in extinction coefficient and quantum yield in response to conjugation and radiolabeling, indicating the ability of the dye to withstand synthesis conditions. A somewhat lower extinction coefficient was observed for ^{68}Ga-M_2 and may be attributable to the presence of acetate buffer in the reaction mixture post-radiolabeling, in contrast to the other samples which were analyzed in water. Nevertheless, the fluorescent signal from ^{68}Ga-M_2 was retained and confirmed by in vivo imaging. Stability studies looking at the radiochemical stability also served as opportunities to confirm fluorescence signal in response to the effects of ^{68}Ga labeling over time.

The conserved fluorescent yield of the NIR fluorophore indicated no significant changes under any of the test conditions and allowed us to proceed to a model of HO where targeting specificity and fluorescent properties of ^{68}Ga-M_2 were assessed in vivo. Qualitatively, a high degree of similarity between pattern and location of new bone formation was observed on both NIR and CT images. Due to the inherent variability of the transduced cell implantations, various degrees of new bone formation were present, but in each case the anatomic rendering of new bone by CT corresponded to the location and relative shape of the functional image from NIR fluorescence. The mouse in Figure 7A and B had a smaller bone mass as shown by the day 11 CT, whereas the mouse in Figure 7C and D had much larger bone formation. Variation in size was evident as early as day four by NIRF imaging and preceded the anatomical appearance of bone by CT.

The rationale for acquiring PET images at 1 h post-injection was based on the rapid clearance of the tracer from circulation via the kidneys and absence of non-specific binding. However, the PET images did not support the NIR findings as poor accumulation of ^{68}Ga-M_2 was observed at sites of HO. Our prior experiments with ^{64}Cu-M_2 required delayed imaging (18 h post-injection) due to high levels of background, liver, and gut uptake at early time points, but could clearly delineate new bone formation by PET.[26] The discrepancies between the PET findings in both studies may be attributed to changing of the radiometal from ^{64}Cu to ^{68}Ga. A study evaluating various somatostatin octapeptides radiolabeled with $^{67/68}Ga$, ^{111}In, and Yttrium-90 (^{90}Y) found that changing the radiometal does indeed cause variation in receptor-binding affinities, cellular internalization rates, hepatic clearance, and in vivo pharmacology.[42] This can result from different conformations of metal–chelator complex, or differences in labeling schemes (i.e., pH or heat) that may impact the peptide adversely. We initially suspected that our imaging time point was premature for detecting tracer localization, however, upon examining the effect of $^{nat/68}Ga$ on M_2 in enzyme binding assays, it was determined that the presence of metal played a key role in outcome of the PET studies. The enzyme binding assays showed a dramatic reduction in affinity of ^{nat}Ga-M_2 compared with unlabeled M_2. Further examination using M_2 that was processed under labeling conditions in the absence of $^{nat}Ga/^{68}Ga$ (i.e., acetate buffer and heat) revealed a 10-fold decrease in enzyme binding affinity compared with unprocessed agent. This may explain the differences between the NIR and PET images in the context of peptide amount used for labeling. In our studies, we selected 6 nmol of peptide (1) for sufficient labeling yield and (2) to provide fluorescent signal for delayed NIR imaging. Under these conditions there is a mixture of ^{68}Ga-M_2, which poorly binds MMP-9, along with a large excess of non-radioactive (processed) M_2 that still retains binding potential. Therefore, the drastic differences in binding affinity and selection of imaging time points may have contributed to the positive signal observed in NIR imaging and the absence of signal on PET.

Our plan to substitute ^{68}Ga for ^{64}Cu did not yield comparable imaging findings. A change in composition to replace DOTA with 1,4,7-triazacyclononane-1,4,7-triacetic acid (NOTA) as the chelator may offer an effective alternative since NOTA possesses a different coordination structure and can label ^{68}Ga at ambient temperature. The NOTA-bioconjugate may have a different affinity profile observed with the metal-bound complex and eliminate any negative effects that resulted from heating. Increasing the radiospecific activity may also minimize differential effects from radioactive and non-radioactive components. Nonetheless, the in vivo findings demonstrate the feasibility of generating and applying a dual-labeled probe with ^{68}Ga and NIRF for multimodality PET/NIRF imaging.

4. Conclusions

We prepared a dual-labeled MMP-9 targeting peptide using ^{68}Ga and IRDye 800CW. The addition of multiple reporters to a targeting agent has the ability to enhance each modality, but also requires additional testing and validation to ensure the agent is stable across biologic, chemical, radiochemical and optical criteria. The dual-conjugate in this study showed excellent stability and retention of optical properties. ^{68}Ga labeling methods were developed and optimized to yield a dual-labeled peptide for PET/NIRF imaging which had excellent radiochemical stability. This study showed that ^{68}Ga labeling conditions did not adversely affect the optical properties of IRDye 800CW and that this strategy can be applied to other dual-labeled peptides and other NIR fluorophores. Modification with a different bifunctional chelator may be useful for further evaluation of the peptide by PET/CT/NIRF imaging in models of HO.

5. Experimental procedures

5.1. Reagents

All reagents were purchased from commercial sources and used without further purification. Chelex-100 resin was purchased from Bio-Rad Laboratories (Richmond, CA) and used with all aqueous buffers to ensure metal-free conditions. A commercially-available $^{68}Ge/^{68}Ga$ generator was purchased from Eckert & Ziegler (Berlin, Germany). Analytical high-performance liquid chromatography (HPLC) was performed on a Hitachi LaChrom system equipped with a 2.6 μm Kinetex C-18 column (Phenomenex, Torrance, CA) with a mobile phase of A = 0.1% TFA in H_2O, B = 0.1% TFA in CH_3CN; gradient, 0 min = 10% B, 10 min = 90% B; flow rate, 1 mL/min. Radio-thin-layer chromatography (radio-TLC) was carried out on a AR-2000 scanner (Bioscan, Washington, DC) using instant thin-layer chromatography (ITLC) strips and 1:1 methanol/0.1 M ammonium acetate. Molecular weight measurement was carried out by ESI on a Waters UPLC system equipped with a Waters PDA detector and a Waters TQD mass spectrometer.

5.2. Peptide synthesis

The DOTA (1,4,7,10-tetraazacyclotetradecane-N',N'',N''',N''''-tetraacetic acid)-modified cyclic MMP-targeting peptide (lactam 2,10) DOTA-KKAHWGFTLD (M_1) was synthesized by New England Peptide (Gardner, MA) according to standard Fmoc-protocols. The peptide was made on a low load Rink amide resin (~0.3 mmol/g, NovaBiochem) using HCTU as the coupling agent. A three-dimensional orthogonal strategy developed by Kates et al.[43] for making cyclic lactam peptides on resin with allyl-based side-chain protection was utilized. The C-terminal Asp was added as the Fmoc-Asp(OAll)-OH derivative, the Lys^2 residue was added as

Fmoc-Lys(Alloc)-OH, and the N-terminal Lys was added as Fmoc-Lys(Boc)-OH and the N-terminal Fmoc group was left on the peptide. After chain assembly, the allyl-based protection was remove from Lys^2 and Asp^{10} using catalytic $Pd(PPh_3)_4$ and excess phenylsilane (~5 equiv relative to allyl-based protection). Cyclization was accomplished with PyClock (2 equiv) with DIPEA (4 equiv) in DMF. The N-terminal Fmoc was removed and DOTA-tris (*t*-Bu ester) (Macrocyclics, Dallas, TX) was added to the N-term. The peptide was cleaved with 90% TFA and purified by reversed-phase chromatography to >95% purity.

5.3. Conjugation of IRDye 800CW

In order to generate a peptide with two reactive amine groups for conjugation to DOTA and IRDye 800CW, we modified the HWGF peptide sequence described by Wang et al. by adding an additional lysine to the N-terminus of the peptide followed by DOTA-conjugation by solid phase synthesis to yield the cyclic decapeptide M_1. Conjugation of IRDye 800CW (LICOR Biosciences, Lincoln, NE) was performed by adding 1.52 mg (1.3 μmol) of dye to a stirred solution of M_1 (2 mg, 1.3 μmol) in 0.1 M sodium phosphate buffer (pH 8.33). The reaction was carried out at 4 °C overnight and the crude mixture was purified with a 2000 MWCO Sartorius Vivaspin spin column (VWR International) or semi-preparative-HPLC to yield M_2.

5.4. MMP-9 binding assays

To examine the binding of the modified peptides, 10 ng of purified MMP-9 (AnaSpec, San Jose, CA) was preincubated with (a) M_2, (b) M_2 processed in non-radioactive labeling conditions (i.e., acetate buffer and heat), or (c) ^{nat}Ga-M_2 for 1 h at concentrations ranging from 100 nM to 500 μM. Excess peptide was separated from enzyme-peptide complex by non-reducing SDS gel electrophoresis and the fluorescent signal of the bound complex was detected by scanning with the Odyssey Infrared Imaging System (LICOR Biosciences, Lincoln, NE). The binding of M_1 and M_2 were compared in a blocking study. MMP-9 (10 ng) was incubated with increasing concentrations of M_1 (200 nM–1 mM) for 1 h. M_2 (2 μM) was then added and incubated for 1 h followed by analysis using non-reducing SDS gel electrophoresis as described above.

5.5. Radiolabeling

^{68}Ga-M_2 was prepared by eluting a 10 mCi $^{68}Ge/^{68}Ga$ generator with 0.1 N HCl and collecting the 2 mL peak fraction. The eluted $^{68}GaCl_3$ was buffered to pH 4 with solid NaOAc. The effects of peptide concentration, buffer concentration, and heating time were tested to determine optimal labeling conditions. Different peptide amounts were added to 0.1 M or 1.25 M NaOAc buffer (pH 4) with reaction volumes ranging from 150 to 710 μL. Samples were heated at 95 °C for 5–20 min. For pharmacological studies, 1 N NaOH (30 μL) was used to adjust to pH 7. Radiochemical purity was assessed by radio-TLC and confirmed by radio-HPLC.

5.6. Synthesis of ^{nat}Ga-M_2

^{nat}Ga-M_2 was synthesized based on conditions developed with ^{68}Ga. M_2 (150 μg, 60 nmol) was mixed with an excess of non-radioactive Ga and the reaction was heated at 95 °C for 13 min. The crude mixture was HPLC purified and characterized by mass spectrometry.

5.7. Stability studies

The chemical, radiochemical and optical stability of radioactive and non-radioactive M_2 were examined using a series of in vitro stability studies. M_2 was incubated in PBS and water at room temperature and 4 °C for 14 days, followed by HPLC analysis of peptide and fluorescent stability. To assess radiochemical stability, ^{68}Ga-M_2 was added to a solution of PBS or DTPA (500-fold excess), kept at room temperature for 1, 2 and 3 h, and analyzed by radio-HPLC. To evaluate serum stability, 150 μL of ^{68}Ga-M_2 was added to 50% mouse serum and incubated at 37 °C. An 80 μL aliquot was taken at each of the above-mentioned time points and added to 160 μL ice-cold acetonitrile. The samples were centrifuged at 14,000 rpm for 5 min and the supernatant was collected, filtered and analyzed by radio-HPLC.

5.8. Determination of log *P* value

The lipophilicity of ^{68}Ga-M_2 was assessed by determination of the water–octanol partition coefficient. 1-Octanol (1 mL) was added to a solution of approximately 25 μCi of ^{68}Ga-M_2in water (1 mL) and the layers were vigorously mixed for 5 min at room temperature. The tubes were centrifuged at 14,000 rpm for 2–3 min. Three samples of 100 μL of each layer were taken in pre-weighed vials, re-weighed, and counted in a γ-counter (Wizard-2, Perkin Elmer). The partition coefficient was determined by calculating the ratio of counts per minute (cpm) in weight (g) of octanol/cpm in weight (g) of water and expressed as log *P*. At least three independent experiments were performed in triplicate to give the log *P* as the mean value ± standard deviation (SD).

5.9. Characterization of fluorescent properties

Fluorescence intensity of the fluorophores was determined using the Fluorolog Tau-3 Spectrofluorometer (Horiba JobinYvon, Edison, NJ) with excitation from a xenon arc lamp and absorbance was recorded using the DU-800 Spectrophotometer (Beckman Coulter, Brea CA). Fluorescence excitation and emission spectra were obtained at wavelengths of 785 and 830 nm, respectively, with an integration time of 0.3 s for 1 μM solutions of IRDye 800CW, M_2 and ^{68}Ga-M_2 ($n = 4$). Fluorescence measurements for IRDye 800CW and M_2 were performed in aqueous solution under ambient conditions, whereas ^{68}Ga-M_2 was prepared as previously described in NaOAc (pH 4) to provide an accurate representation of the ^{68}Ga-labeling scheme. Extinction coefficients were determined from the slope of absorbance at 785 nm as a function of the concentration of serial dilutions of each agent. Fluorescence quantum yield was determined by the comparative method of Williams et al.[44] using the quantum yield of ICG ($\Phi = 0.016$) at 785/830 nm as a standard.

5.10. Quantitation of BMP2 protein and activity from adenovirus transduced MRC cells

The culture supernatant was collected after transduction with AdHM4 (control) or AdBMP2 in MRC5 cells at 2,500 vp/cell and BMP-2 protein levels assessed using an AP assay.[45] W20-17 cells were assayed for AP activity 72 h after the addition of conditioned culture supernatant or various known concentrations of recombinant BMP-2. A Student's t-test was applied to demonstrate significance.

5.11. Animal model

All animal studies were performed in accordance with the standards of Baylor College of Medicine (Houston, TX), Department of Comparative Medicine and The University of Texas Health Science Center (Houston TX), Center for Molecular Imaging after review and approval of the protocol by their respective Institutional Animal Care and Use Committee (IACUC) or Animal

Welfare Committee (AWC). A murine model of BMP-2 induced HO was used by transducing human fibroblast (MRC5) cells with either Adempty (control) or AdBMP2, followed by intramuscular injection into each hind limb quadriceps muscle of non-obese diabetic/severely compromised immunodeficient (NOD/SCID) mice. Control transduced cells were injected into the contralateral limb. The data showed that elevated RNA protein expression and active MMP-9 content in tissues injected with AdBMP2 transduced cells were maximal four days after implantation and were significantly elevated when compared to the contralateral tissues receiving Adempty transduced cells.

5.12. In vivo imaging

Based on the findings from the ex vivo analysis, mice ($n = 3$) were imaged on day four post-implantation with multimodality imaging to assess localization and in vivo fluorescence of M_2 following ^{68}Ga-labeling. For all imaging procedures, mice were anesthetized with 1% isoflurane. μPET/CT imaging was performed on day four post-implantation using a Siemens Inveon μPET/CT scanner (Siemens Medical, Knoxville, TN) with instrument parameters as previously described.[14] The anesthetized mice were injected intravenously with ^{68}Ga-M_2 (200 μCi, 6 nmol) and μPET/CT images were acquired 1 h post-injection. To visualize the formation of ectopic bone, CT imaging was performed on days 4 and 11 post-implantation.

NIR fluorescence images were acquired 18 h after intravenous administration of ^{68}Ga-M_2 using a custom-built fluorescence imaging systems previously described.[2] Briefly, a field of view was illuminated with 785 nm of light from a laser diode, outfitted with a convex lens and diffuser to create a uniform excitation field. The fluorescence was collected through holographic and interference filters placed before a Nikon camera lens. The images were finally captured by an electron-multiplying charge-coupled device camera (PhotonMax 512; Princeton Instruments, Princeton, NJ) with 200–400 ms of integration time. For acquisition of white-light images, the optical filters were removed, and a low-power lamp illuminated the subject. Image acquisition was accomplished by V++ software (Auckland, New Zealand).

Acknowledgments

The authors acknowledge Robert P. Hammer (New England Peptide) for his technical assistance with design and synthesis of the peptide conjugate. This work was supported by Defense Advanced Research Projects Agency W911NF-09-1-0040 and Department of Defense W81XWH-07-0281 (EO-D) and W81XWH-07-1-025 (EO-D).

References and notes

1. Culver, J.; Akers, W.; Achilefu, S. *J. Nucl. Med.* **2008**, *49*, 169.
2. Houston, J. P.; Ke, S.; Wang, W.; Li, C.; Sevick-Muraca, E. M. *J. Biomed. Opt.* **2005**, *10*, 054010.
3. Sevick-Muraca, E. M.; Rasmussen, J. C. *J. Biomed. Opt.* **2008**, *13*, 041303.
4. Marshall, M. V.; Rasmussen, J. C.; Tan, I.-C. A. M. B.; Adams, K. E.; Wang, X.; Fife, C. E.; Maus, E. A.; Smith, L. A.; Sevick-Muraca, E. M. *Open Surg. Oncol. J.* **2010**, *2*, 12.
5. Adams, K. E.; Ke, S.; Kwon, S.; Liang, F.; Fan, Z.; Lu, Y.; Hirschi, K.; Mawad, M. E.; Barry, M. A.; Sevick-Muraca, E. M. *J. Biomed. Opt.* **2007**, *12*, 024017.
6. Sampath, L.; Wang, W.; Sevick-Muraca, E. M. *J. Biomed. Opt.* **2008**, *13*, 041312.
7. Sampath, L.; Kwon, S.; Ke, S.; Wang, W.; Schiff, R.; Mawad, M. E.; Sevick-Muraca, E. M. *J. Nucl. Med.* **2007**, *48*, 1501.
8. Chen, Y.; Dhara, S.; Banerjee, S. R.; Byun, Y.; Pullambhatla, M.; Mease, R. C.; Pomper, M. G. *Biochem. Biophys. Res. Commun.* **2009**, *390*, 624.
9. Liu, Z.; Liu, S.; Niu, G.; Wang, F.; Chen, X. *Mol. Imaging* **2010**, *9*, 21.
10. Wang, W.; Ke, S.; Wu, Q.; Charnsangavej, C.; Gurfinkel, M.; Gelovani, J. G.; Abbruzzese, J. L.; Sevick-Muraca, E. M.; Li, C. *Mol. Imaging* **2004**, *3*, 343.
11. Tanaka, E.; Choi, H. S.; Humblet, V.; Ohnishi, S.; Laurence, R. G.; Frangioni, J. V. *Surgery* **2008**, *144*, 39.
12. Cao, Q.; Liu, S.; Niu, G.; Chen, K.; Yan, Y.; Liu, Z.; Chen, X. *Amino Acids* **2010**.
13. Ogawa, M.; Regino, C. A.; Seidel, J.; Green, M. V.; Xi, W.; Williams, M.; Kosaka, N.; Choyke, P. L.; Kobayashi, H. *Bioconjug. Chem.* **2009**, *20*, 2177.
14. Sampath, L.; Kwon, S.; Hall, M. A.; Price, R. E.; Sevick-Muraca, E. M. *Transl. Oncol.* **2010**, *3*, 307.
15. Becker, A.; Hessenius, C.; Licha, K.; Ebert, B.; Sukowski, U.; Semmler, W.; Wiedenmann, B.; Grotzinger, C. *Nat. Biotechnol.* **2001**, *19*, 327.
16. Achilefu, S.; Jimenez, H. N.; Dorshow, R. B.; Bugaj, J. E.; Webb, E. G.; Wilhelm, R. R.; Rajagopalan, R.; Johler, J.; Erion, J. L. *J. Med. Chem.* **2002**, *45*, 2003.
17. Li, C.; Wang, W.; Wu, Q.; Ke, S.; Houston, J.; Sevick-Muraca, E.; Dong, L.; Chow, D.; Charnsangavej, C.; Gelovani, J. G. *Nucl. Med. Biol.* **2006**, *33*, 349.
18. Edwards, W. B.; Xu, B.; Akers, W.; Cheney, P. P.; Liang, K.; Rogers, B. E.; Anderson, C. J.; Achilefu, S. *Bioconjug. Chem.* **2008**, *19*, 192.
19. Kimura, R. H.; Miao, Z.; Cheng, Z.; Gambhir, S. S.; Cochran, J. R. *Bioconjug. Chem.* **2010**.
20. Chang, Y. H.; Lin, I. L.; Tsay, G. J.; Yang, S. C.; Yang, T. P.; Ho, K. T.; Hsu, T. C.; Shiau, M. Y. *Clin. Biochem.* **2008**, *41*, 955.
21. Lancelot, E.; Amirbekian, V.; Brigger, I.; Raynaud, J. S.; Ballet, S.; David, C.; Rousseaux, O.; Le Greneur, S.; Port, M.; Lijnen, H. R.; Bruneval, P.; Michel, J. B.; Ouimet, T.; Roques, B.; Amirbekian, S.; Hyafil, F.; Vucic, E.; Aguinaldo, J. G.; Corot, C.; Fayad, Z. A. *Arterioscler. Thromb. Vasc. Biol.* **2008**, *28*, 425.
22. Muroski, M. E.; Roycik, M. D.; Newcomer, R. G.; Van den Steen, P. E.; Opdenakker, G.; Monroe, H. R.; Sahab, Z. J.; Sang, Q. X. *Curr. Pharm. Biotechnol.* **2008**, *9*, 34.
23. Boschetto, P.; Quintavalle, S.; Zeni, E.; Leprotti, S.; Potena, A.; Ballerin, L.; Papi, A.; Palladini, G.; Luisetti, M.; Annovazzi, L.; Iadarola, P.; De Rosa, E.; Fabbri, L. M.; Mapp, C. E. *Thorax* **2006**, *61*, 1037.
24. Deryugina, E. I.; Quigley, J. P. *Cancer Metastasis Rev.* **2006**, *25*, 9.
25. Manduca, P.; Castagnino, A.; Lombardini, D.; Marchisio, S.; Soldano, S.; Ulivi, V.; Zanotti, S.; Garbi, C.; Ferrari, N.; Palmieri, D. *Bone* **2009**, *44*, 251.
26. Rodenberg, E.; Azhdarinia, A.; Lazard, Z.; Hall, M.; Kwon, S.; Wilganowski, N.; Merched-Sauvage, M.; Salisbury, E. A.; Davis, A. R.; Sevick-Muraca, E. M.; Olmsted-Davis, E. Submitted for publication (copy on file with author).
27. Koivunen, E.; Arap, W.; Valtanen, H.; Rainisalo, A.; Medina, O. P.; Heikkila, P.; Kantor, C.; Gahmberg, C. G.; Salo, T.; Konttinen, Y. T.; Sorsa, T.; Ruoslahti, E.; Pasqualini, R. *Nat. Biotechnol.* **1999**, *17*, 768.
28. Kuhnast, B.; Bodenstein, C.; Haubner, R.; Wester, H. J.; Senekowitsch-Schmidtke, R.; Schwaiger, M.; Weber, W. A. *Nucl. Med. Biol.* **2004**, *31*, 337.
29. Sprague, J. E.; Li, W. P.; Liang, K.; Achilefu, S.; Anderson, C. J. *Nucl. Med. Biol.* **2006**, *33*, 227.
30. Hanaoka, H.; Mukai, T.; Habashita, S.; Asano, D.; Ogawa, K.; Kuroda, Y.; Akizawa, H.; Iida, Y.; Endo, K.; Saga, T.; Saji, H. *Nucl. Med. Biol.* **2007**, *34*, 503.
31. Wang, W.; Shao, R.; Wu, Q.; Ke, S.; McMurray, J.; Lang, F. F., Jr.; Charnsangavej, C.; Gelovani, J. G.; Li, C. *Mol. Imaging Biol.* **2009**, *11*, 424.
32. Poeppel, T. D.; Krause, B. J.; Heusner, T. A.; Boy, C.; Bockisch, A.; Antoch, G. *Eur. J. Radiol.* **2009**, *70*, 382.
33. Cronin, C. G.; Swords, R.; Truong, M. T.; Viswanathan, C.; Rohren, E.; Giles, F. J.; O'Dwyer, M.; Bruzzi, J. F. A. J. R. *Am. J. Roentgenol.* **2010**, *194*, W91.
34. Kuil, J.; Velders, A. H.; van Leeuwen, F. W. *Bioconjug. Chem.* **2010**, *21*, 1709.
35. Hofmann, M.; Maecke, H.; Borner, R.; Weckesser, E.; Schoffski, P.; Oei, L.; Schumacher, J.; Henze, M.; Heppeler, A.; Meyer, J.; Knapp, H. *Eur. J. Nucl. Med.* **2001**, *28*, 1751.
36. Maecke, H. R.; Hofmann, M.; Haberkorn, U. *J. Nucl. Med.* **2005**, *46*(Suppl 1), 172S.
37. Virgolini, I.; Ambrosini, V.; Bomanji, J. B.; Baum, R. P.; Fanti, S.; Gabriel, M.; Papathanasiou, N. D.; Pepe, G.; Oyen, W.; De Cristoforo, C.; Chiti, A. *Eur. J. Nucl. Med. Mol. Imaging* **2010**, *37*, 2004.
38. Velikyan, I.; Beyer, G. J.; Langstrom, B. *Bioconjug. Chem.* **2004**, *15*, 554.
39. Breeman, W. A.; de Jong, M.; de Blois, E.; Bernard, B. F.; Konijnenberg, M.; Krenning, E. P. *Eur. J. Nucl. Med. Mol. Imaging* **2005**, *32*, 478.
40. Zhernosekov, K. P.; Filosofov, D. V.; Baum, R. P.; Aschoff, P.; Bihl, H.; Razbash, A. A.; Jahn, M.; Jennewein, M.; Rosch, F. *J. Nucl. Med.* **2007**, *48*, 1741.
41. Meyer, G. J.; Macke, H.; Schuhmacher, J.; Knapp, W. H.; Hofmann, M. *Eur. J. Nucl. Med. Mol. Imaging* **2004**, *31*, 1097.
42. Antunes, P.; Ginj, M.; Zhang, H.; Waser, B.; Baum, R. P.; Reubi, J. C.; Maecke, H. *Eur. J. Nucl. Med. Mol. Imaging* **2007**, *34*, 982.
43. Kates, S. A.; Solé, N. A.; Johnson, C. R.; Hudson, D.; Barany, G.; Albericio, F. *Tetrahedron Lett.* **1993**, *34*, 1549.
44. Williams, A. T. R.; Winfield, S. A.; Miller, J. N. *Analyst* **1983**, *108*, 1067.
45. Olmsted, E. A.; Blum, J. S.; Rill, D.; Yotnda, P.; Gugala, Z.; Lindsey, R. W.; Davis, A. R. *J. Cell. Biochem.* **2001**, *82*, 11.